



## Physical and Electrical Characterization of ZrO<sub>2</sub> Gate Insulators Deposited on Si(100) Using Zr(O<sup>i</sup>-Pr)<sub>2</sub>(thd)<sub>2</sub> and O<sub>2</sub>

H.-W. Chen,<sup>a,z</sup> T.-Y. Huang,<sup>a,b</sup> D. Landheer,<sup>c,\*</sup> X. Wu,<sup>c</sup> S. Moisa,<sup>c</sup> G. I. Sproule,<sup>c</sup> and T.-S. Chao<sup>b,d</sup>

<sup>a</sup>Institute of Electronics Engineering, National Chiao-Tung University, Hsinchu 300, Taiwan

<sup>b</sup>National Nano Device Laboratories, Hsinchu 300, Taiwan

<sup>c</sup>Institute for Microstructural Sciences, National Research Council of Canada, Ottawa, Ontario K1A 0R6, Canada

<sup>d</sup>Department of Electrophysics, National Chiao-Tung University, Hsinchu 300, Taiwan

The characteristics of ultrathin ZrO<sub>2</sub> films deposited using molecular oxygen and the zirconium precursor Zr(O<sup>i</sup>-Pr)<sub>2</sub>(thd)<sub>2</sub> [where O<sup>i</sup>-Pr is isopropoxide and thd is 2,2,6,6-tetramethyl-3,5-heptanedionate] were investigated. The organometallic was dissolved as a 0.15 M solution in octane and introduced into the deposition chamber using a liquid injection system. The deposition rate was insensitive to molecular oxygen flow but changed with liquid injection rate and was thermally activated in the range 390-550°C. No evidence of Zr-C and Zr-Si bonds were found in the X-ray photoelectron spectroscopy (XPS), spectra, and carbon concentrations, <0.1 atom %, the detection limit of the XPS depth profiling measurements, were obtained at the lowest deposition temperatures and deposition rates. High-resolution transmission electron microscopy showed the ZrO<sub>2</sub> films to be polycrystalline as deposited, with an amorphous zirconium silicate interfacial layer. The effects of postdeposition annealing were also demonstrated. After proper annealing treatments, promising capacitance-voltage and current-voltage characteristics were achieved. A film with an equivalent oxide thickness of 2.3 nm showed current reductions of approximately two orders of magnitude when compared to SiO<sub>2</sub>, but some improvements are required if these films are to be used as a gate-insulator beyond the 100 nm CMOS (complementary metal oxide semiconductor) technology node.

© 2002 The Electrochemical Society. [DOI: 10.1149/1.1471891] All rights reserved.

Manuscript submitted August 31, 2001; revised manuscript received December 2, 2001. Available electronically April 12, 2002.

As the dimensions of complementary metal oxide semiconductor (CMOS) devices are scaled in the deep submicrometer regime, the thickness of the required gate dielectric will steadily decrease to dimensions <1 nm.<sup>1</sup> For SiO<sub>2</sub>, however, the large resulting direct tunneling currents result in large power consumption and reduced reliability.<sup>2,3</sup> With higher dielectric constant,  $\kappa$ , the gate insulator thickness can increase, while maintaining the equivalent oxide thickness (EOT), significantly reducing the tunneling leakage current. Recently, high- $\kappa$  materials predicted to be thermodynamically stable with Si,<sup>4</sup> such as ZrO<sub>2</sub>, HfO<sub>2</sub>, La<sub>2</sub>O<sub>3</sub>, Al<sub>2</sub>O<sub>3</sub>, and their silicates, have been considered as candidates for alternative gate dielectrics.<sup>5</sup> ZrO<sub>2</sub> has a high dielectric constant (~25), high bandgap energy (5.8-7.8 eV),<sup>5,6</sup> and thermal compatibility with contemporary CMOS processes.<sup>7-9</sup>

Although electron-beam evaporation or sputtering are useful techniques for depositing new materials for evaluation, they can damage electrical devices, have difficulties with uniformity and purity, and are hard to maintain in production, resulting in low throughput. Thus, chemical vapor deposition (CVD) is usually preferred and, in this paper, organometallic CVD (MOCVD) was used to deposit ZrO<sub>2</sub>. Since zirconium chloride (ZrCl<sub>4</sub>)<sup>10</sup> and alkoxide [Zr(O<sup>i</sup>-Bu)<sub>4</sub> and Zr(O<sup>i</sup>-Pr)<sub>4</sub>]<sup>9,11,12</sup> precursors contain an unsaturated four coordinate Zr<sup>IV</sup> center, they are air and moisture sensitive. For zirconium  $\beta$ -diketonates [e.g., Zr(acac)<sub>4</sub>, Zr(thd)<sub>4</sub>, and Zr(tfac)<sub>4</sub>], the chelating ligand ( $\beta$ -diketonate) can increase the coordination number of Zr<sup>IV</sup> center to eight to achieve the coordination saturation. Although it makes the Zr coordination compound less ambient sensitive, the compound has higher thermal stability, requiring higher deposition temperatures, and films exhibit severe carbon or fluorine contamination.<sup>12,13</sup> Thus, a mature MOCVD process requires precursors, stable upon exposure to atmosphere with higher vapor pressure, to replace the chloride or alkoxide precursors usually employed. Most recently, the anhydrous zirconium nitrate Zr(NO<sub>3</sub>)<sub>4</sub> was also investigated for gate dielectrics.<sup>14-17</sup>

In order to combine the advantages of alkoxides and  $\beta$ -diketonates, the mixed ligand zirconium precursor was developed to lower the thermal stability but with the higher ambient stability and higher volatility. This paper reports the first investigation of the physical and electrical properties of ultrathin ZrO<sub>2</sub> films deposited using molecular oxygen and a recently developed six-coordinate mixed alkoxide/ $\beta$ -diketonate compound, Zr(O<sup>i</sup>-Pr)<sub>2</sub>(thd)<sub>2</sub> (O<sup>i</sup>-Pr is isopropoxide and thd is 2,2,6,6-tetramethyl-3,5-heptanedionate),<sup>18</sup> introduced into the chamber with a liquid injection system. The films were analyzed by high-resolution transmission electron microscopy (HRTEM) and X-ray photoelectron spectroscopy (XPS). Pure, stoichiometric ZrO<sub>2</sub> films were deposited and the effects of postdeposition annealing investigated. Low leakage current density vs. voltage (J-V) characteristics and capacitance-voltage (C-V) characteristics with small hysteresis are demonstrated.

### Experimental

Si(100) substrates, 100 mm diam, n-type ( $\rho = 0.02$ - $0.06 \Omega \text{ cm}$ ) were given an HF-last RCA clean prior to film deposition. The CVD chamber was equipped with a 360 L/s turbomolecular pump and a liquid injection system (LDS-300B produced by ATMI). The latter consisted of a liquid pump to pump the precursor, a 0.15 M solution of Zr(O<sup>i</sup>-Pr)<sub>2</sub>(thd)<sub>2</sub> in octane, through a hot glass frit at a rate of 0.2 mL/min. The vapors were carried with a 50 sccm flow of Ar to a gas distribution ring 10 cm from the substrate. The glass frit, the components of the vaporizer, the gas ring, and the connecting tube were maintained at a temperature of 190°C with heating tapes and blankets, while the substrate temperature was controlled in the range 390-550°C with quartz-halogen lamps and a thermocouple. Oxygen was introduced into the chamber at flow rates of 0-150 sccm through a separate gas distribution ring 30 cm from the substrate. Just prior to deposition the wafers were heated for 10 min at 500°C in 10 mTorr O<sub>2</sub> to replace the surface hydrogen termination with oxygen.

Films were analyzed by X-ray photoelectron spectroscopy (XPS) using a PHI 5500 system with a monochromatic Al K $\alpha$  X-ray source in a standard 90° geometry (X-ray source and electron spectrometer 45° off normal) and a bandpass energy of 58.7 eV. Depth profiling was accomplished with intermittent Ar<sup>+</sup> sputtering at 1 keV, 50

\* Electrochemical Society Active Member.

<sup>z</sup> E-mail: hwchen.ee86g@nctu.edu.tw

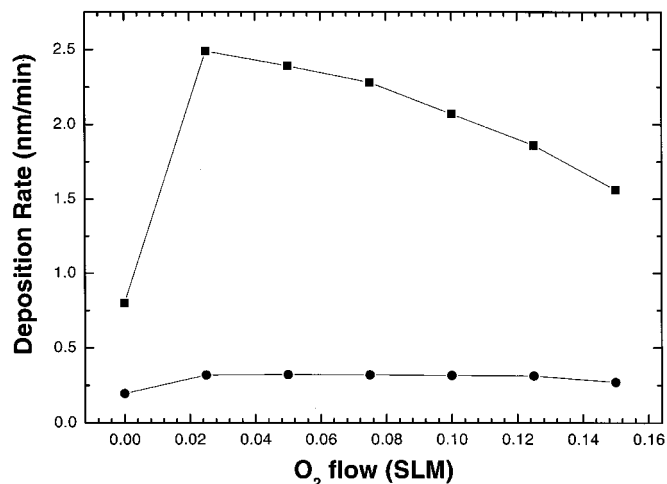


**Figure 1.** The deposition rate vs. oxygen flow for films deposited in continuous mode at (●) 500 and (■) 650°C. The precursor was injected at 0.05 mL/min with 50 sccm Ar.

nA, and 45° incidence. Thick films were typically stoichiometric  $\text{ZrO}_2$  when analyzed by Rutherford backscattering. These were used to calibrate the sensitivity factors for the XPS analysis of thinner films using the Zr 3d and O 1s peaks. The peak positions were referenced to the main surface carbon peak at 284.8 eV.

Since the liquid pump was not sufficiently stable at flow rates below 0.2 mL/min, to reduce deposition rates and further reduce the carbon contamination, most depositions were done in “pulse mode” in which the precursor and oxygen were introduced separately with intervening pumping periods of 15 s. Nitrogen at a flow rate of 100 sccm was introduced into the oxygen gas ring and flowed during the complete deposition cycle. Thus, each cycle of deposition consisted of four stages: 100 sccm  $\text{N}_2$ , 150 sccm  $\text{O}_2$  + 100 sccm  $\text{N}_2$ , 100 sccm  $\text{N}_2$ , and 50 sccm Ar + 100 sccm  $\text{N}_2$  + Zr precursor (0.2 mL/min). Pressures at various stages of the deposition cycle were in the 8–12 mTorr range.

The depositions were monitored *in situ* with a Rudolph i1000 ellipsometer operating at a wavelength of 633 nm. The ellipsometric angles were used to calculate the deposited film thickness in real-

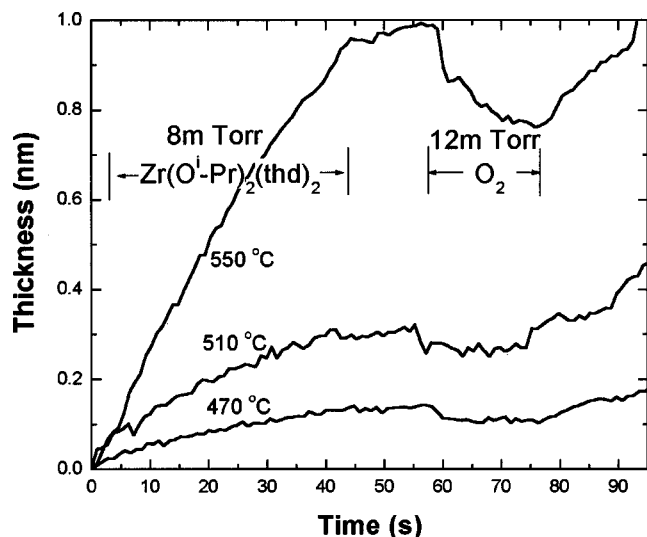


**Figure 2.** Film thickness as a function of time obtained from the *in situ* ellipsometer during one cycle of deposition for substrate temperatures 470, 510, and 550°C.

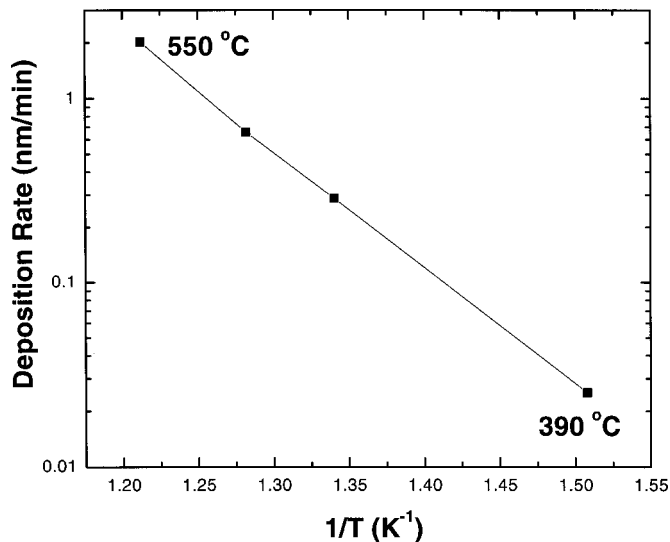


**Figure 3.** Logarithmic plot of the deposition rate vs. inverse temperature. The activation energy determined from the slope is 1.27 eV.

time from the known optical constants for Si and assuming the film was uniform, nonabsorbing, and had a refractive index of 2. This results in an approximate thickness measurement that must be calibrated by *ex situ* analysis.

Atomic force microscopy (AFM) measurements were made on the as-deposited and annealed samples using a Digital Instruments Nanoscope III operating in tapping mode with 5 nm diam silicon probes. Cross-sectional samples were made using a low-angle ion-milling technique. The structure of the films and the effect of annealing was observed directly in HRTEM micrographs made on a Philips EM-430T instrument operating at 250 keV.

Samples were annealed in a Heatpulse 610 (Steag RTP Systems) rapid thermal processor. For spike anneals in  $\text{O}_2$ , the temperature was ramped at 125°C/s to 800, 850, 900, or 950°C and held for 1 s before the quartz lamps were turned off. Forming gas anneals (FGAs) were done in a 4%  $\text{H}_2$  in  $\text{N}_2$  mixture for 10–30 min in the temperature range 380–600°C.

For the electrical measurements, Al-gated capacitors were made by evaporating aluminum through a shadow mask and back contacts were made with In-Ga eutectic. The FGAs were done before metal deposition to avoid reaction of the Al with the films. The area of the capacitors was measured to an accuracy of  $\pm 2\%$  with a calibrated digitizing camera. Electrical measurements were made by probing the Al gates in a probe-station attached to two instruments, a multi-frequency LCR meter (HP model 4275A) for C-V characteristics, and a picoammeter/dc voltage source (HP model 4140B) for current-voltage characteristics. High-frequency C-V measurements were made by stepping with 0.1 V steps each second, first from  $-2.5$  to  $+2.5$  V and then in the reverse direction to look for hysteresis. The equivalent oxide thickness EOT was obtained from the 100 kHz C-V characteristics by using the NCSU C-V fitting routine,<sup>19</sup> which includes quantum effects in the channel.

## Results and Discussion

**Physical characteristics.**—Initial films were deposited in the continuous mode in which the oxygen and precursor were introduced simultaneously. Figure 1 shows the deposition rate as a function of oxygen flow rate for depositions at 500 and 650°C using a continuous flow of precursor of 0.05 mL/min. The deposition rate is insensitive to molecular oxygen flow at 500°C; however, turning off the oxygen does significantly reduce the deposition rate at both temperatures. With an oxygen flow of 100 sccm the deposition rate was proportional to precursor flow rate over the range of 0.05–0.20 mL/

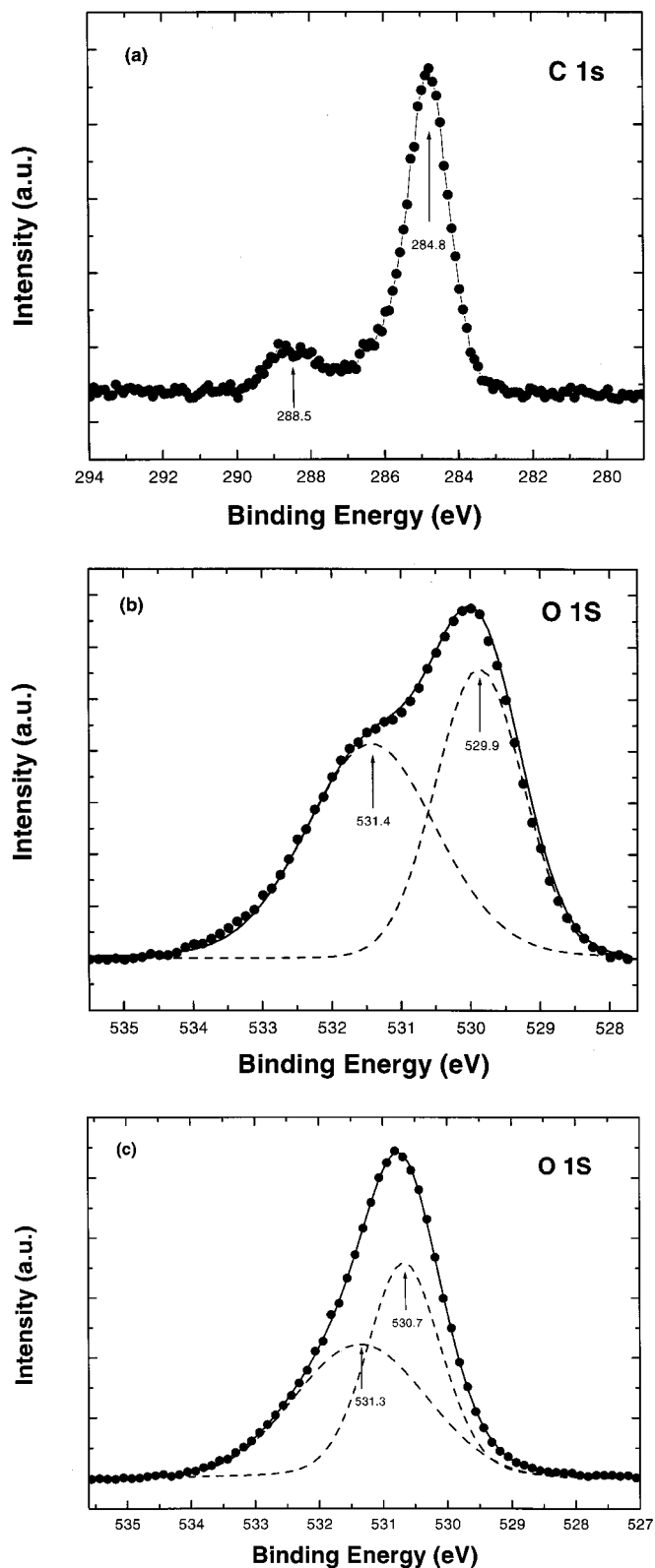


**Figure 4.** XPS spectra showing data (●) and (---) fitted peaks for the  $\text{ZrO}_2$  film deposited with 75 cycles at  $390^\circ\text{C}$ : (a) C 1s (surface), (b) O 1s (surface), and (c) O 1s (after two cycles of sputtering). The solid lines are a guide to the eye in (a) and represent the sum of the fitted peaks in (b) and (c).

min. Depth profiles of the C 1s peaks showed that the films deposited in the continuous mode were contaminated with carbon, with the smallest contamination in the 1-2 atom % range, which is consistent with the value reported in Ref. 12 at the lower temperature where the deposition rates were lowest.

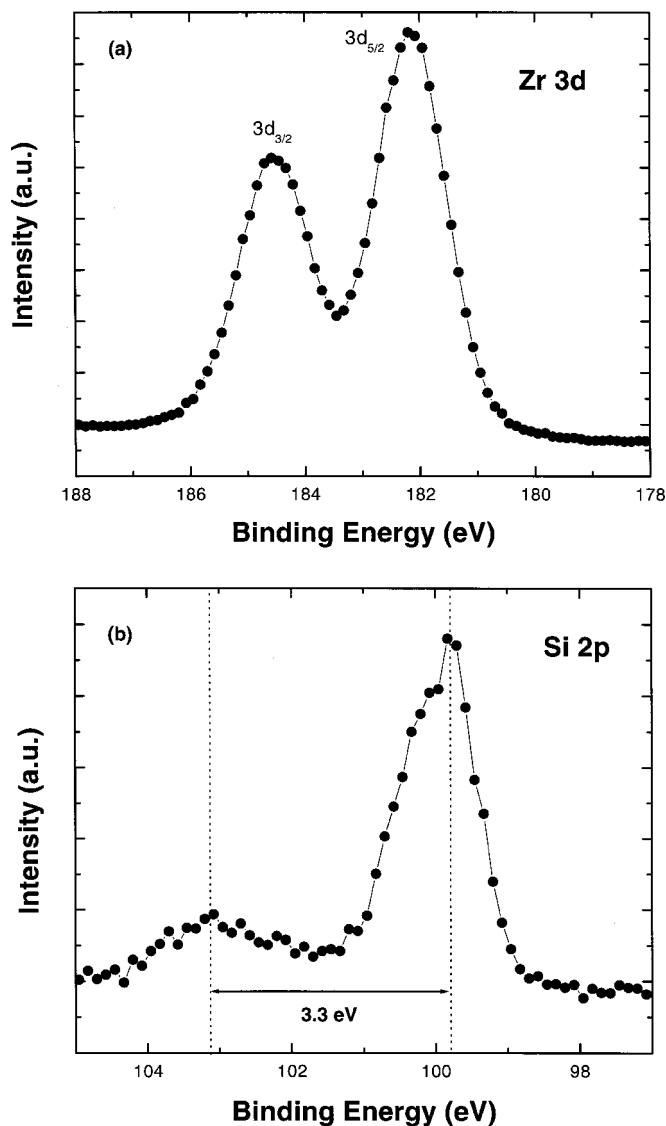


**Figure 5.** More XPS spectra for the film of Fig. 4: (a) Zr 3d peak, and (b) Si 2p peak. In (b) the peak near 103 eV shifted 3.3 eV from the substrate peak is associated with a silicate layer at the Si interface. The solid curves are a guide to the eye.

Carbon concentrations tended to be lower for the lowest pump rates, but subsequent depositions were done at 0.20 mL/min to avoid periodic instabilities in the pumping rate caused by back-pressure instabilities in the liquid injection pump at the lower speeds. To reduce carbon contamination, subsequent depositions were done in the pulse mode.

For our flow parameters, the film thickness depends on the number of deposition cycles, substrate temperature,  $\text{O}_2$  injection time, and precursor injection time during pulse-mode deposition. In the range of temperature and pressure investigated here no saturation of the precursor absorption was noted, *i.e.*, the film deposition rate did not saturate as the precursor injection time was increased. Furthermore, when the oxygen was turned off the deposition rate did not decrease significantly in the pulse mode. This indicates that atomic layer deposition (ALD) was not occurring, possibly because back-ground oxygen from the process was sufficient to effect the oxidation. Since the Zr is coordinated to six oxygens in the precursor, it is also possible that an oxidant is not necessary to form  $\text{ZrO}_2$ . However, without oxygen the carbon in the films was significant, so films were typically deposited with an oxygen injection time of 18 s and

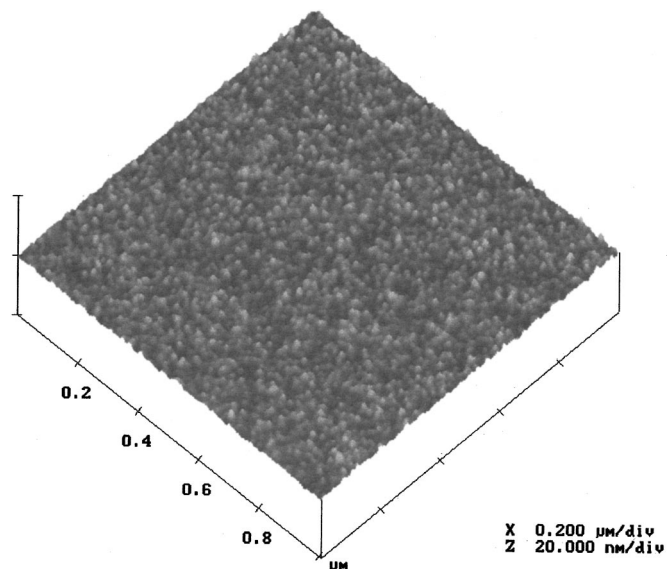


**Figure 6.** AFM image for the film of Fig. 4. The rms surface roughness is 4.4 Å.

a precursor injection time of 43 s. With this “pulse mode” deposition, O<sub>2</sub> can react with the film and reduce the carbon in the film effectively.

The thickness output by the *in situ* ellipsometer during one cycle is shown in Fig. 2 for substrate temperatures of 470, 510, and 550°C. The film thickness increases during the precursor injection but seems to decrease during oxygen flow. The latter decrease is recovered during the subsequent pump-down (period with nitrogen flow only) and may be associated with adsorption and desorption of oxygen on the surface. A plot of the log of the average deposition rate as a function of inverse temperature is shown in Fig. 3. The activation energy determined from the slope of the fit to the data in the range 390–550°C is 1.27 eV.

In Fig. 4, the XPS C 1s (surface), O 1s (surface), and O 1s (after two cycles of sputtering) spectra for the ZrO<sub>2</sub> film deposited with 75 cycles at 390°C are shown. The C 1s spectrum of Fig. 4a reveals carbon peaks at binding energies of 284.8 and 288.5 eV, corresponding to C-C and C-O bonds, respectively. No lower binding energy peak characteristic of the Zr-C bond was found. After two cycles of sputtering these peaks disappeared in the films deposited at 390 and 470°C, indicating that the carbon concentrations in these films were less than the detection limit of our instrument, *i.e.*, <0.1 atom %.

Guittet *et al.*<sup>20</sup> found the binding energy,  $E_b$ , for the O 1s peak to be  $E_b = 530.0$  eV for ZrO<sub>2</sub> and  $E_b = 531.3$  eV for ZrSiO<sub>4</sub>. These energies are close to the fitted components of the O 1s spectra shown in both Fig. 4b and c. In Fig. 4b, the O 1s spectrum of the as-deposited film has a component peak at the binding energy of 531.4 eV. Because the O 1s binding energies of the Zr silicate, hydroxide, and carbonate are in the same range<sup>21</sup> as the higher energy peak, some of this peak in Fig. 4b is due to the H-O and C-O bonds from remnant precursor and from water vapor adsorbed during transfer to the XPS system. After two cycles of sputtering, the O 1s spectrum, shown in Fig. 4c, has a main peak with binding energy of 530.7 eV, close to that expected for ZrO<sub>2</sub>. The higher energy peak appearing in Fig. 4b is diminished because there is no water vapor and the residual carbon in the film is <0.1 atom %. Its binding energy of 531.3 eV is associated with the Zr-O-Si bonds in the interfacial layer.

Figure 5a shows the Zr 3d spectrum of the same ZrO<sub>2</sub> film deposited with 75 cycles at 390°C. No evidence of Zr-Si bond formation is observed from Fig. 5a. The binding energy difference  $E_b$  (O 1s)- $E_b$  (Zr 3d<sub>5/2</sub>) = 348.4 eV is close to the value of 348.1 eV

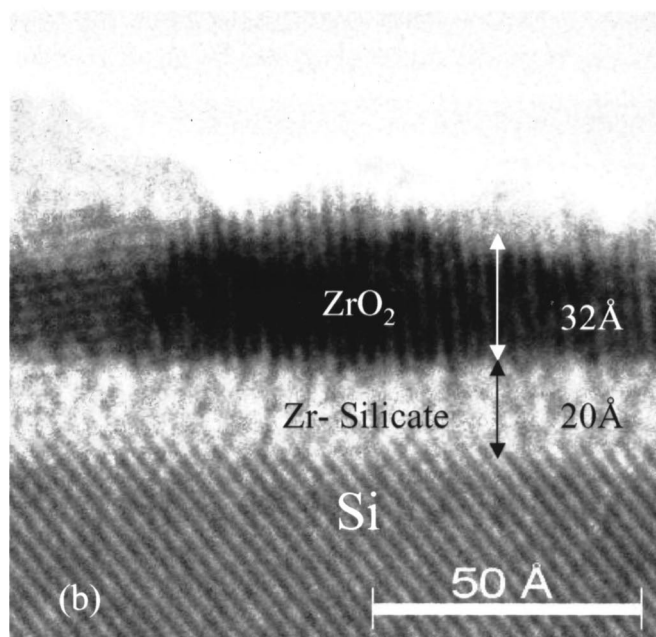
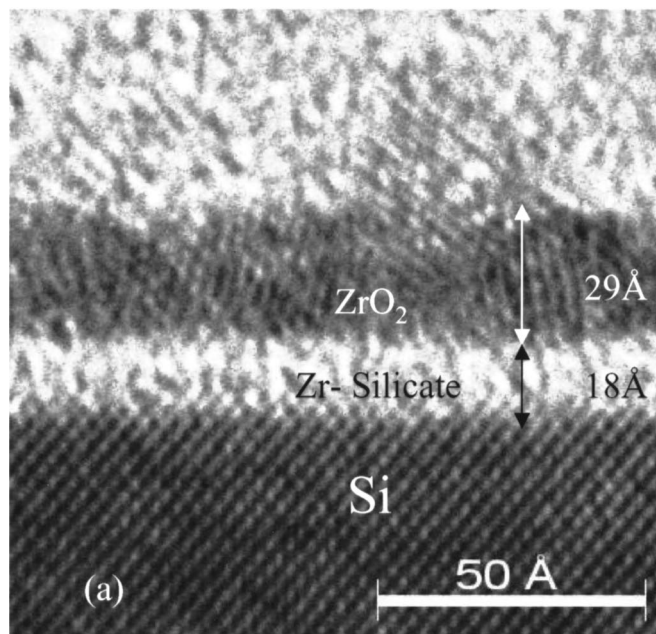


**Figure 7.** HRTEM cross-sectional images of the film of Fig. 4: (a) as-deposited, (b) after spike anneal at 850°C for 1 s in O<sub>2</sub> followed by FGA at 380°C for 20 min.

reported in Ref. 20. Figure 5b shows the Si 2p spectrum of the same sample shown in Fig. 5a. The peak near the binding energy of ~103 eV is 3.3 eV from the Si substrate peak, a chemical shift smaller than the >4 eV shift observed for 1.8 nm thick SiO<sub>2</sub> films.<sup>22</sup> This is characteristic of a silicate layer consistent with the TEM image and C-V data shown later. In addition, the residual carbon contamination for this film is less than the detection limit. The root mean square (rms) surface roughness obtained from the AFM image of the same film (shown in Fig. 6) is 4.4 Å.

In Fig. 7a and b, an amorphous interfacial layer is evident between the substrate and the polycrystalline ZrO<sub>2</sub> layer in the HRTEM image of the film. This layer is identified as the silicate layer responsible for the Si 2p feature in the XPS spectrum. The interface between silicate and Si is atomically sharp. After spike

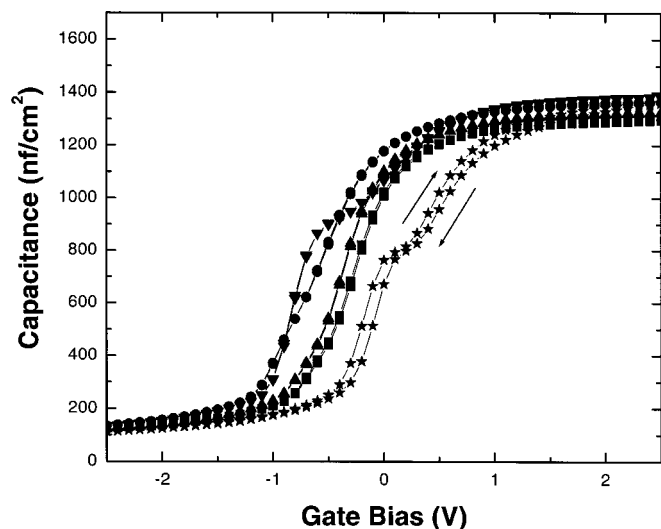
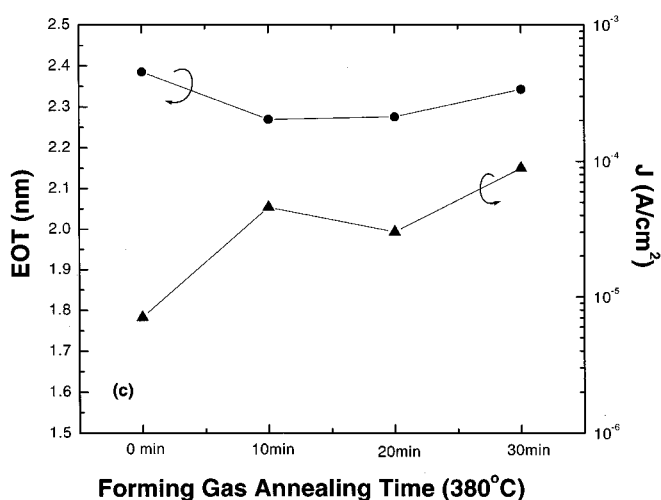
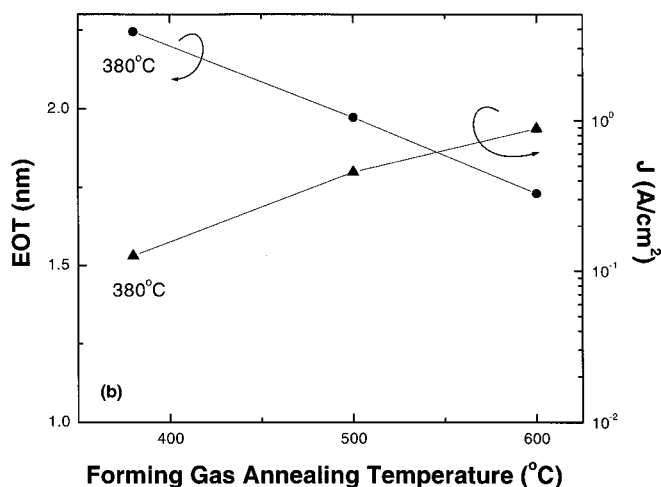
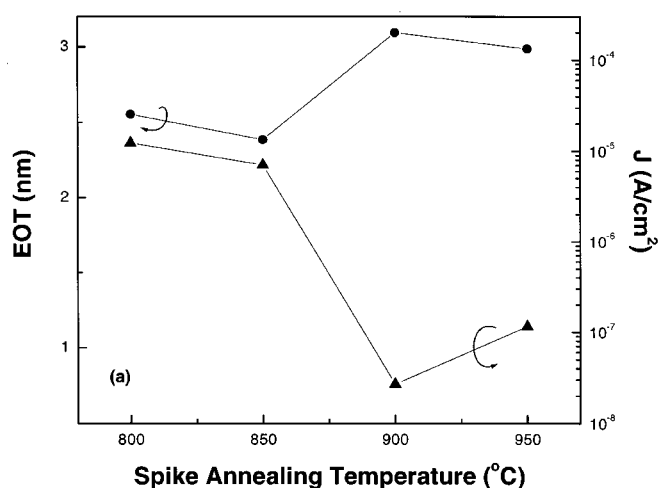


**Figure 8.** High-frequency C-V characteristics of capacitors with  $\text{ZrO}_2$  gate dielectrics obtained at 100 kHz. The samples were spike annealed for 1 s in  $\text{O}_2$  at  $850^\circ\text{C}$  first, then annealed in forming gas at  $380^\circ\text{C}$  for 10-30 min: (- $\star$ -) no anneals, (- $\nabla$ -) spike anneal only, (- $\bullet$ -) 10 min FGA, (- $\blacktriangle$ -) 20 min FGA, and (- $\blacksquare$ -) 30 min FGA.

anneal in  $\text{O}_2$  at  $850^\circ\text{C}$  and FGA, the thickness of the silicate layer was increased by 2 Å, as shown in Fig. 7b. This is due to oxygen penetration to the Si substrate since  $\text{ZrO}_2$  is a fast ion conductor with significant oxygen ion diffusivity.<sup>6</sup> The most likely mechanism for silicate formation is that the oxygen reacted with the Si substrate to grow  $\text{SiO}_2$ , and  $\text{SiO}_2$  reacted with  $\text{ZrO}_2$  to form Zr silicate. Films were grown without injecting oxygen and, as stated previously, this did not significantly reduce the film deposition rate. It also did not reduce the thickness of the interfacial silicate layer, further indication that oxygen released from the precursor is available for surface reactions.

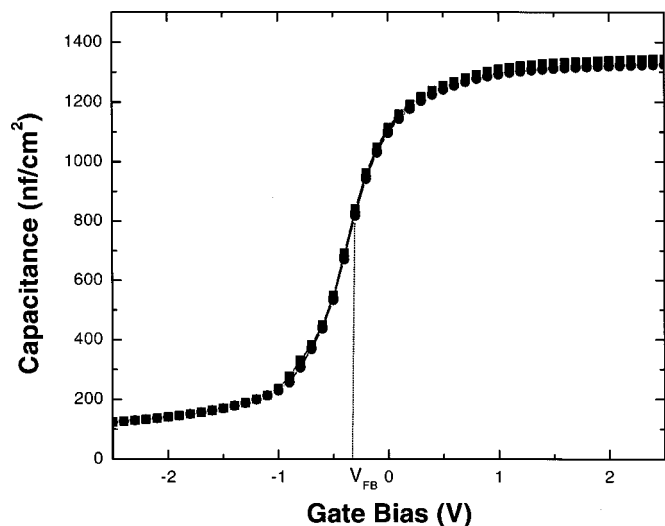
**Electrical characteristics.**—Electrical analysis was performed on the  $\text{ZrO}_2$  film formed with 75 deposition cycles at  $390^\circ\text{C}$ . The 100 kHz C-V characteristics of  $\text{ZrO}_2$  films deposited are shown in Fig. 8 for different annealing treatments. For the as-deposited sample, there is a significant hump in the C-V curve in accumulation, a flatband voltage  $V_{\text{FB}} = -0.06$  V (scan from inversion to accumulation), corresponding to a large negative fixed charge density ( $N_f = -1.1 \times 10^{12}/\text{cm}^2$ ), and a significant clockwise hysteresis given by  $\Delta V_{\text{FB}} \sim 0.21$  V. The hysteresis is associated with an effective density of trapped charge at the interface,  $\Delta N_t = -1.7 \times 10^{12}/\text{cm}^2$ , attributed to charge trapping or detrapping. It is believed that the appearance of the hump is due to  $P_b$  centers at the interface.<sup>23</sup> For the sample spike annealed for 1 s in  $\text{O}_2$  at  $850^\circ\text{C}$ , the flatband voltage shifts to  $-0.76$  V ( $N_f = 6.0 \times 10^{12}/\text{cm}^2$ ), the hysteresis becomes smaller, but the hump still exists. Thus  $\text{O}_2$  annealing reduces the charge trapping-detrapping (to  $\Delta N_t \sim -1.6 \times 10^{11}/\text{cm}^2$ ) but does not passivate the  $P_b$  centers effectively.

The samples annealed in forming gas at  $380^\circ\text{C}$  were first spike annealed at  $850^\circ\text{C}$  for 1 s in  $\text{O}_2$ . For these samples the  $P_b$  centers are passivated. For the 20 min FGA,  $\Delta N_t$  is reduced to  $5.0 \times 10^{10}/\text{cm}^2$ . For the 30 min FGA the flatband voltage shifts toward the ideal flatband voltage (for this sample, ideal  $V_{\text{FB}} = W_{\text{ms}} \sim -0.2$  V, where  $W_{\text{ms}}$  is the work function difference).<sup>24</sup> The fixed charge density is reduced to  $2.6 \times 10^{11}/\text{cm}^2$ . This may be due to the introduction of negative fixed charge or the annealing of the positive fixed charge. However, the hysteresis is increased to  $\Delta N_t = -5.5 \times 10^{10}/\text{cm}^2$ , so there appears to be a trade-off between trapped and fixed charge.



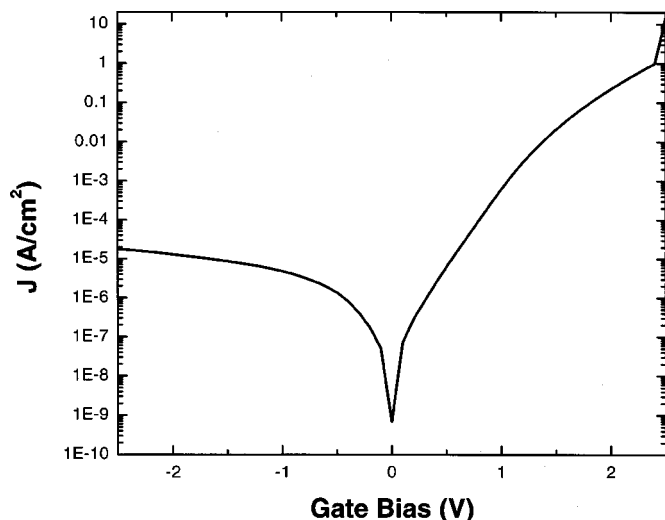
**Figure 9.** The variation of EOT and gate current density ( $J$ ) as a function of postdeposition annealing treatments. (a) 1 s spike anneal in  $\text{O}_2$  at  $850^\circ\text{C}$  from 800 to  $950^\circ\text{C}$ , (b) FGA from 380 to  $600^\circ\text{C}$  for 10 min, and (c) spike anneal for 1 s in  $\text{O}_2$  at  $850^\circ\text{C}$  first, then FGA at  $380^\circ\text{C}$  for 10-30 min; (- $\bullet$ -) EOT, and (- $\blacktriangle$ -)  $J$  for  $V_G - V_{\text{FB}} = 1$  V.

Figure 9 shows the variation of the EOT and the gate current density,  $J$ , after different postdeposition annealing treatments. The value of  $J$  was obtained at a value of gate voltage,  $V_G$ , for which  $V_G - V_{\text{FB}} = 1$  V. The EOT of the as-deposited  $\text{ZrO}_2$  film is 27 Å, so



**Figure 10.** Frequency dependence of the C-V characteristics of the film of Fig. 4 which has an EOT of 2.27 nm after spike anneal at 850°C in O<sub>2</sub> for 1 s and FGA at 380°C for 20 min: (—■—) 10 and (---●---) 100 kHz. A slight frequency dispersion is evident below midgap. The hysteresis ( $\Delta V_{FB} \approx 6$  mV) is not shown.

either spike anneal or FGA can make the EOTs lower, *i.e.*, the effective dielectric constant of the whole gate dielectric becomes higher. As shown in Fig. 9a, the EOT is without significant change at 800-850°C and increases at 900-950°C. The increase of EOT at the highest spike annealing temperatures is associated with the oxygen penetration to the Si substrate, which increases the interfacial layer thickness as mentioned above. The accompanying reduction of the leakage current is due to the larger physical thickness and the improved robustness of the ZrO<sub>2</sub> films. However, the samples only treated with FGA are quite different, as shown in Fig. 9b. The leakage current increases with the FGA temperature, and the EOT shows a tendency to decline. The increasing leakage current might be related to the leaky path via the ZrO<sub>2</sub> polycrystalline grain boundaries created by forming gas. In Fig. 9c, the EOT is essentially unchanged after FGAs for 10-30 min, and the changes may be due entirely to variations in film thickness over the wafer. However, the increase in



**Figure 11.** Current density as a function of gate voltage for the sample in Fig. 10.

leakage current for the 30 min FGA is larger than expected from the variation in EOT, and this may again be related to hydrogen effects on the grain boundaries.

Figure 10 shows the 10 kHz and 100 kHz C-V curves of the ZrO<sub>2</sub> capacitor treated with spike annealing at 850°C for 1 s in O<sub>2</sub> followed by FGA at 380°C for 20 min. The area of the capacitor is  $6.6 \times 10^{-4}$  cm<sup>2</sup>. From the 100 kHz C-V curve, the EOT is 22.7 Å with the quantum effects correction. The effective dielectric constant of the whole dielectric layer is  $\sim 9.3$ , which is lower than that of ZrO<sub>2</sub> because the equivalent oxide capacitance is dominated by the capacitance of the silicate layer. In addition, there is only slight frequency dispersion in the C-V curves, mainly below midgap. This indicates that frequency-dependent interface states are passivated during the annealing. The interface state density is estimated to be  $5.0 \times 10^{11}$  cm<sup>-2</sup> eV<sup>-1</sup> by the method described in Ref. 25, which compares the 10 kHz and ideal C-V characteristics.

As shown in Fig. 11, the J-V curve for the sample in Fig. 10 is asymmetric. The leakage characteristics were measured under light illumination to avoid the minority carrier generation current limiting the leakage current at inversion. The leakage current densities are  $6 \times 10^{-4}$  A/cm<sup>2</sup> at 1 V (substrate injection) and  $4.7 \times 10^{-6}$  A/cm<sup>2</sup> at -1 V (gate injection), respectively. For a pure SiO<sub>2</sub> film with a EOT 22.7 Å, the leakage current density is about two orders of magnitude larger for a gate potential  $V_G = V_{FB} + 1$  V.<sup>3</sup> However, the leakage is larger than expected from tunneling and does not fit the equations for Frenkel-Poole emission or Schottky emission.<sup>26</sup> This might be due to the difference of the barrier heights under different voltage polarity or might be due to a peaked distribution of traps in the dielectric that favors trap-assisted tunneling for substrate injection.<sup>27</sup> Further investigation of the leakage mechanism is necessary, but reducing the film surface roughness observed by HRTEM and AFM should improve performance.

## Conclusions

Ultrathin stoichiometric, carbon-free ZrO<sub>2</sub> films can be deposited on Si(100) using the novel precursor Zr(O<sup>i</sup>-Pr)<sub>2</sub>(thd)<sub>2</sub> dissolved in octane. O<sub>2</sub> introduced into the chamber is necessary to reduce the carbon contamination. In XPS data, no evidence of Zr-C and Zr-Si bonds were found. Meanwhile, XPS and HRTEM analysis shows that a Zr silicate layer is formed at the interface during deposition. Although the silicate layer reduces the effective dielectric constant of the gate dielectrics, it may provide a better and more stable interface with Si, reducing the interface state density. It could also improve the carrier mobility in the channel of a MOSFET<sup>8</sup> (metal oxide semiconductor field effect transistor) by providing a smoother interface in direct contact with the Si substrate. However, the thickness of this silicate layer must be reduced to meet future CMOS technology requirements.

The continuous-mode deposition data of Fig. 1 indicate that deposition rates do decrease when the oxygen is turned off, and this indicates that there may be a regime where growth saturates if the layers are not fully oxidized. Thus, ALD may be possible with this precursor if the pumping system were changed to allow higher pressures during the gas pulses with shorter pumping cycles characteristic of classical ALD. This might also result in thinner silicate layers since the total exposure of the silicon surface to oxygen might be reduced.

The thin ZrO<sub>2</sub> films exhibit good C-V and J-V characteristics. After proper annealing treatments, an EOT of 22.7 Å was achieved with a leakage current about two orders of magnitude lower than that of SiO<sub>2</sub> with the same EOT. The P<sub>b</sub> centers in the ZrO<sub>2</sub> films were effectively passivated by FGA. The slight remnant frequency dispersion below midgap might be reduced if a proper FGA were performed after, rather than before, gate electrode definition. These electrical properties demonstrate that thin ZrO<sub>2</sub> films formed by Zr(O<sup>i</sup>-Pr)<sub>2</sub>(thd)<sub>2</sub> and O<sub>2</sub> might be a promising gate dielectric material for deep-submicrometer CMOS devices if the roughness of the layers and the thickness of the interfacial layer can be reduced. In

addition, it might be plausible to apply the thin  $ZrO_2$  films in flash memory as the gate dielectric over the floating gate to increase the coupling ratio. However, further investigations of its reliability are indispensable before using this  $ZrO_2$  film process in CMOS technology.

### Acknowledgments

The authors are grateful to Dr. Shioh-Huey Chuang at National Nano Device Laboratories for her fruitful discussion. We also acknowledge E. Estwick and T. Quance for assistance in the preparation of the samples. In addition, we thank Dr. J. R. Hauser for use of the NCSU C-V analysis program. This work was supported by the National Science Council of the Republic of China under contract no. NSC89-2215-E-009-071.

*The National Chiao-Tung University assisted in meeting the publication costs of this article.*

### List of Symbols

$E_b$	binding energy
$J$	gate current density
$N_f$	fixed charge density
$V_{FB}$	flatband voltage
$V_G$	gate voltage
$W_{ms}$	work function difference

Greek

$\Delta N_t$	effective density of trapped charge
$\Delta V_{FB}$	flatband voltage shift
$\kappa$	dielectric constant of film

### References

1. *The International Technology Roadmap for Semiconductors*, Semiconductor Industry Association, San Jose, CA (2000).
2. S.-H. Lo, D. A. Buchanan, Y. Taur, and W. Wang, *IEEE Electron Device Lett.*, **18**, 209 (1997).
3. B. Brar, G. D. Wilk, and A. C. Seabaugh, *Appl. Phys. Lett.*, **69**, 2728 (1996).
4. D. J. Hubbard and D. G. Schlom, *J. Mater. Res.*, **11**, 2757 (1996).
5. G. D. Wilk, R. M. Wallace, and J. M. Anthony, *J. Appl. Phys.*, **89**, 5243 (2001).
6. J. Robertson, *J. Vac. Sci. Technol. B*, **18**, 1785 (2000).
7. W.-J. Qi, R. Nieh, B. H. Lee, L. Kang, Y. Jeon, K. Onishi, T. Ngai, S. Banerjee, and J. C. Lee, *Tech. Dig. Int. Electron Devices Meet.*, **1999**, 145.
8. W.-J. Qi, R. Nieh, B. H. Lee, K. Onishi, L. Kang, Y. Jeon, J. C. Lee, V. Kaushik, B. Y. Nguyen, L. Prabhu, K. Eisenbeiser, and J. Finder, *Symposium on VLSI Technology*, IEEE, p. 40 (2000).
9. C.-H. Lee, H. F. Luan, W. P. Bai, S. J. Lee, T. S. Jeon, Y. Senzaki, D. Roberts, and D. L. Kwong, *Tech. Dig. Int. Electron Devices Meet.*, **2000**, 27.
10. M. Copel, M. Gribelyuk, and E. Gusev, *Appl. Phys. Lett.*, **76**, 436 (2000).
11. Q. Lu, R. Lin, P. Ranade, Y.-C. Yeo, X. Meng, H. Takeuchi, T.-J. King, C. Hu, H. Luan, S. Lee, W. Bai, C.-H. Lee, D.-L. Kwong, X. Guo, X. Wang, and T.-P. Ma, *Tech. Dig. - Int. Electron Devices Meet.*, **2000**, 641.
12. A. C. Jones, *Chem. Vap. Deposition*, **4**, 169 (1998).
13. S. B. Desu, T. Shi, and C. K. Kowk, *Mater. Res. Soc. Symp. Proc.*, **168**, 349 (1990).
14. D. G. Colombo, D. C. Glimmer, V. G. Young, Jr., S. A. Campbell, and W. L. Gladfelter, *Chem. Vap. Deposition*, **4**, 220 (1998).
15. R. C. Smith, N. Hoilien, C. J. Taylor, T. Ma, S. A. Campbell, J. T. Roberts, M. Copel, D. A. Buchanan, M. Gribelyuk, and W. L. Gladfelter, *J. Electrochem. Soc.*, **147**, 3472 (2000).
16. R. C. Smith, T. Ma, N. Hoilien, L. Y. Tsung, M. J. Bevan, L. Colombo, J. Roberts, S. A. Campbell, and W. L. Gladfelter, *Adv. Mater. Opt. Electron.*, **10**, 105 (2000).
17. T. Ma, S. A. Campbell, R. Smith, N. Hoilien, B. He, W. L. Gladfelter, C. Hobbs, D. Buchanan, C. Taylor, M. Gribelyuk, M. Tiner, M. Copel, and J. J. Lee, *IEEE Trans. Electron Devices*, **48**, 2348 (2001).
18. A. C. Jones, T. J. Leedham, P. J. Wright, M. J. Crosbie, P. A. Lane, D. J. Williams, K. A. Fleeting, D. J. Otway, and P. O'Brien, *Chem. Vap. Deposition*, **4**, 46 (1998).
19. J. R. Hauser and K. Ahmed, in *Characterization and Metrology for ULSI Technology, 1998 International Conference*, D. G. Seiler, A. C. Diebold, W. M. Bullis, T. J. Shaffner, R. McDonald, and E. J. Walters, Editors, pp. 235-239, The American Institute of Physics, Woodbury, NY (1998).
20. J. Guittet, J. P. Crocombette, and M. Gautier-Soyer, *Phys. Rev. B*, **63**, 125117 (2001).
21. M. J. F. Moulder, W. F. Stickle, P. E. Sobol, K. D. Bomben, and J. Chastain, *Handbook of X-Ray Photoelectron Spectroscopy*, p. 45, Perkin-Elmer Corporation, Eden Prairie, MN (1992).
22. S. Iwata and I. Akitoshi, *J. Appl. Phys.*, **79**, 6653 (1996).
23. P. Lundgren and M. O. Andersson, *J. Appl. Phys.*, **74**, 4780 (1993).
24. E. H. Nicollian and J. R. Brews, *MOS (Metal Oxide Semiconductor) Physics and Technology*, p. 465, Wiley, New York (1982).
25. L.-Å. Ragnarsson and P. Lundgren, *J. Appl. Phys.*, **88**, 938 (2000).
26. S. M. Sze, *Physics of Semiconductor Devices*, 2nd ed., p. 403, Wiley, New York (1981).
27. M. Houssa, M. Tuominen, M. Naili, V. Afanas'ev, A. Stesmans, S. Haukka, and M. M. Heyns, *J. Appl. Phys.*, **87**, 8615 (2000).